


Steam Oxidation Resistance of Advanced Steels and Ni-Based Alloys at 700 °C for 1000 h

T. Dudziak¹  · K. Jura² · A. Polkowska¹ · V. Deodeshmukh³ · M. Warmuzek¹ · M. Witkowska⁴ · W. Ratuszek⁴ · K. Chruściel⁴

Received: 10 June 2017 / Revised: 24 October 2017 / Published online: 14 November 2017
© The Author(s) 2017. This article is an open access publication

Abstract The aim of the work was to investigate corrosion resistance of highly alloyed steels and Ni-based alloys in a steam atmosphere for 1000 h at 700 °C. In these steam oxidation experiments, two solid solution strengthened alloys; Haynes[®] 230[®], 617 alloy, two gamma-prime (γ') strengthened alloys; 263 and Haynes[®] 282[®] and three Cr+Ni- rich stainless steels: 309S, 310S and HR3C austenitic steels were exposed. The study showed that the materials exposed commonly developed thin oxide scales; in Ni-based alloys, these consisted of mainly MnCr_2O_4 spinels and Cr_2O_3 , with the exception of 617 alloy where NiCr_2O_4 spinels and Cr_2O_3 were found. In Fe-based alloys, Cr_2O_3 , MnCr_2O_4 spinels, $\text{Fe,Mn}(\text{SiO})_4$, and finally Fe_3O_4 developed. No evaporation of chromia has been found within 1000 h test period. Furthermore, the development of TiO_2 was not observed into a large extent in Haynes[®] 282[®] and 263 alloy, in contrast to the study performed at 800 °C under the same steam environment conditions.

Keywords Steam oxidation · Steels · Ni-based alloys · High temperature · XRD

✉ T. Dudziak
tomasz.dudziak@iod.krakow.pl

¹ Foundry Research Institute (FRI), Zakopianska 73, 30-418 Kraków, Poland

² EDF Polska, Ciepłownicza 1, 31-587 Kraków, Poland

³ Haynes International, 1020 West Park Avenue, Kokomo, IN 46904-9013, USA

⁴ Faculty of Metals Engineering and Industrial Computer Science, AGH University Science and Technology, Al. A. Mickiewicza 30, 30-059 Kraków, Poland

Introduction

Coal-fired power plants are one of the key methods of energy production worldwide. However, energy produced from coal emits a large quantity of CO₂ when technology used for energy production is inefficient and old. In the High Efficiency Low Emission (HELE) roadmap for coal technology, prepared by the International Energy Agency (IEA) in 2012, it is proposed that these old and inefficient coal plants fired at subcritical conditions (SbC) should be replaced by new units with higher efficiency for ultra-supercritical conditions (USC) and advanced ultra-supercritical conditions (A-USC) steam parameters [1]. The old technologies called *subcritical conditions* in coal-fired power plants require low pressure and low temperatures [2]. The steam pressure and temperature are adjusted to the steel material used power plant; therefore, low-type T/P22 (2.5 wt% Cr), T/P91 (9 wt% Cr) are used with limited functionality and temperatures of around 600 °C. Their usability is limited due to the formation of thick non-protective oxide scales consisting predominantly of iron oxides. Furthermore, due to large emissions of CO₂ from subcritical power plants, a new law was introduced in the European Union which demanded the reduction of CO₂ by 20–30% by 2020. Nevertheless, electrical energy production from coal will still continue due to economic reasons and the high content of carbon worldwide. However, the energy from coal needs to be produced in a much more efficient manner, using a new generation of coal power plants, where austenitic steels and Ni-based alloys are used in order to withstand harsh conditions at temperatures above 700 °C in super heater (SH) and reheater sections (RH). Currently, attention is paid to austenitic steels and Ni-based alloys with a high Cr content (> 20 wt%) in order to sustain development of continuous, thin, adherent Cr₂O₃ oxides for the extended lifetime of super heaters (SH) and reheaters (RH) systems. Recently, Essuman et al. [3] has found that Ni-based alloys rich in Cr and develops rich Cr scales; however, the Ni-based alloys 105, 263 and 740 exposed at 800 °C underwent an additional deep internal oxidation process. The problem of internal corrosion by oxidation of Al and Ti in grain boundaries is often met in gamma-prime (γ') strengthened alloys [4], and the internal oxidation process is described by Young [5]. The process of oxidation underneath the oxide scale is problematic, especially in the case where a thin and protective oxide layer develops as is often observed in a rich Cr alloys. The alloy infected by internal oxidation, loses its ability to withstand mechanical loads and undergoes accelerated degradation. The internal oxidation process cannot be omitted and neglected, and the process is always observed in structural materials based on γ (Ni) with additions of Ti, Al.

In this work, the study of steam oxidation has been performed on two solid solution strengthened alloys; Haynes[®] 230[®], and 617 alloy, two (γ') gamma-prime strengthened alloys; 263 and Haynes[®] 282[®] and high-alloyed steels rich in Cr: 309S, 310S and HR3C. The materials have been tested under 1 bar pressure in a 100% water–steam–water system at 700 °C for 1000 h.

Experimental Procedures

Steam Oxidation

In this work, for high-temperature oxidation resistance of Ni-based and Fe-based alloys the same rig was used as shown previously [6]. In general, the rig consisted of a heat resistant furnace, where a reaction chamber made of 8 mm thick 316L stainless steel was used, inside the reaction chamber an Al_2O_3 5-mm thick ceramic liner was inserted. The Al_2O_3 liner prevents a steam oxidation reaction with the 316L stainless steel vessel reaction chamber under high-temperature exposures. Hence, the Al_2O_3 liner in this work was responsible for the constant partial pressure of oxygen during high-temperature tests. Deionised water was used throughout the system of polyamide cables and 304L stainless steel tubes and was delivered by a peristaltic pump with 2.833 ml/min flow rate into the system. Throughout the high-temperature tests, deionised water in the reservoir was constantly purged by nitrogen in order to eliminate oxygen dissolved in water from the ambient atmosphere (air). Nitrogen flow was constantly measured by a flow metre connected to the purging line. The samples were placed on the Al_2O_3 ceramic holder and introduced to the furnace. The furnace was locked using four screws made of stainless steel. Further, when the chamber was closed, the nitrogen was run in order to purge the chamber and the samples for 2 h at 200 °C, to remove moisture and other impurities. In the same time, deionised water in the tank was constantly purged. Finally, when temperature was rising to reach the final point, nitrogen flow through the reactive chamber was turned off and the peristaltic pump was turned on to deliver deionised water to the reaction chamber. As mentioned, the tank with deionised water was constantly purged by nitrogen from a cylinder, when the test was finished, during the cooling period; the peristaltic pump was turned off to prevent furnace inundation. Finally, the samples were removed at room temperature (20 °C).

XRD Investigations

The phase analyses have been performed using two techniques; Bragg–Brentano (BB) geometry and the geometry of constant angle known as grazing incidence using $\alpha = 1^\circ$ and $\alpha = 3^\circ$. In Bragg–Brentano (BB) geometry, depth penetration of X-rays can be estimated using the following formula:

$$X = \frac{-\ln(1 - Gx) \sin \theta}{2\mu} \quad (1)$$

where Gx denotes the intensity of the primary X-ray, giving important information related to irradiation volume. μ is the linear absorption coefficient

In the grazing angle method, X-ray depth penetration was calculated via the following formula:

$$X = \frac{-\ln(1 - Gx)}{\left\{ \mu \left[\frac{1}{\sin \alpha} + \frac{1}{\sin(2\theta - \alpha)} \right] \right\}} \quad (2)$$

where Gx denotes the intensity of the primary X-ray, giving important information related to irradiated volume, this value is equivalent to 0.95 (95%). μ is the linear absorption coefficient and, α is the incidence angle.

The calculated values of Gx (assumption of $Gx = 95\%$) were provided in the past [6]

Materials

In this study, seven alloys were exposed; two solid solution strengthened alloys; Haynes[®] 230[®], 617 alloy and two gamma-prime (γ') strengthened materials; 263 alloy and Haynes[®] 282[®] and high-alloyed steels rich in Cr: 309S, 310S and HR3C. Table 1 shows nominal compositions according to producer certificates of the high-alloyed steels and Ni-based alloys, respectively.

Prior to the steam test at 700 °C, materials were cut out from the plate in small squares (20 mm²). As mentioned, HR3C alloy was delivered as a tube section, the material was machined into tube segments, which had dimensions of ~15 mm length, × 10 mm width chord, with a 4-mm wall thickness. The surfaces of the steels and alloys were ground using 600 grit SiC paper. Furthermore, the samples were cleaned in acetone at 40 °C for 20 min using an ultrasonic bath. Prior and during the exposure, the samples were accurately weighed using a digital balance with a resolution of ± 0.01 mg for masses $m = < 80$ g. The digital balance Sartorius CPA225D was calibrated frequently using its internal calibration function and periodically with test weights. The oxidised samples in the first instance were characterised to investigate phase formation using a D500 Kristalloflex with monochromatic X-ray sources Cu ($K = 1.54$ Å), an X-ray diffractometer (XRD) and an EMPYREAN Panalytical X-ray diffractometer with X-ray source Cu using Ni filter. Further steps of post-exposure preparation of the samples after high-temperature testing included, mounting of the samples in the conductive resin from Struers. The mounted samples were ground and polished using TegraPol-35 facility using following SiC papers and time: 220/1; 500/2; 1000/2 min. The polishing procedure of the exposed samples included several steps using diamond suspension: 9 µm/4 min; 3 µm/3 min; 1 µm/3 min; 1/4 µm/3 min that is recommended by Struers for brittle and soft materials. Finally, the ground, polished samples were ultrasonically cleaned for 15 min using TECHPAN TYPE UM-1 machine in alcohol and dried using compressed air. The prepared materials were investigated using: FEI Scios ultra-high-resolution dual-beam scanning electron microscope (SEM) in backscatter electron (BSE) mode, microanalyses were performed using a silicon drift detector (SDD) in energy X-ray spectrometry (EDS) with standard resolution of 127 eV and accelerating voltage 25 kV.

Table 1 Chemical composition of the materials (wt%) used in steam oxidation work

	Ni	Fe	Cr	Co	Mo	Si	Mn	Cu	Nb	La	Ti	Al	C	W	B	P	S	N
309S	14	Bal.	23	-	-	0.75	2	-	-	-	-	-	0.2	-	-	0.045	0.03	-
310S	21	Bal.	25	-	-	1.5	2	-	-	-	-	-	0.08	-	-	0.045	0.03	-
HR3C	20	Bal.	25	-	-	0.75	1.2	-	0.45	-	-	-	0.06	-	-	0.04	0.03	0.2
263 alloy	Bal.	0.6	20	20	6	0.4	0.6	0.2	-	-	1.2	0.6	0.06	-	-	-	-	-
617 alloy	Bal.	1	22	12.5	9	-	-	-	-	-	0.3	1.2	0.07	-	-	-	-	-
Haynes® 230®	Bal.	3	22	5	2	0.4	0.5	-	-	0.02	-	0.3	0.1	14	0.015	-	-	-
Haynes® 282®	Bal.	1.5	20	10	8.5	0.15	0.3	-	-	-	2.1	1.5	0.06	-	0.05	-	-	-

Results

Oxidation Behaviour

Mass gain versus time for steels and Ni-based alloys exposed for 1000 h at 700 °C in steam-rich atmosphere is shown in Figs. 1 and 2, respectively.

The obtained data show that the mass gain of austenitic steels is slightly higher than that achieved by Ni-based alloys. The highest mass gain has been found in HR3C and 309S steels (around 0.32 and 0.31 mg/cm²), whereas the lowest mass gain has been found in solid solution strengthened alloy Haynes[®] 230[®] (around 0.14 mg/cm²). In both cases, the exposed austenitic steels and Ni-based alloys showed no exfoliation, scale spallation during the high-temperature exposure at 700 °C for 1000 h. In comparison to the results presented for 800 °C, 1000 h, the exposed materials at 700 °C showed the formation of much lower mass gain (mg/cm²) as is shown in Table 2, in some cases even four times lower (Haynes[®] 282[®]). In general, much lower mass gain compared to the results at 800 °C was achieved for Ni-based alloys (around 3–4 times lower mass gain) than for austenitic steels (2 times lower mass gain). The results clearly indicate that austenitic steels are more susceptible to temperature changes than Ni-based alloys. At 800 °C, 309SS, 310Ss and HR3C showed lower mass gain than alloy 263 and Haynes[®] 282[®]; however at 700 °C, all steel showed higher mass gains when compared to Ni-based alloys.

The data shown in Figs. 3 and 4 present the exponent *n* factor calculations for austenitic steels and Ni-based alloys, respectively. The performed evaluation using log mass gain versus log time dependence indicates that Ni-based alloys showed nearly parabolic rate behaviour with *n* = 0.4–0.5 [7]. The austenitic steels with high Cr content showed large a deviation in terms of parabolic mechanism, with an *n* factor of 0.1–0.2. Low *n* factor represents an influence and take into account the deviation of the oxidation reaction at an early stage of the process. These

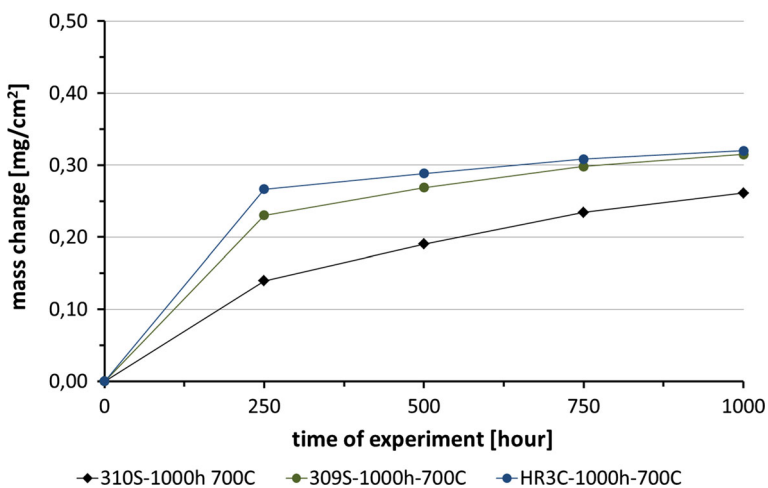


Fig. 1 Kinetic data of the advanced steels exposed to steam oxidation regime at 700 °C for 1000 h

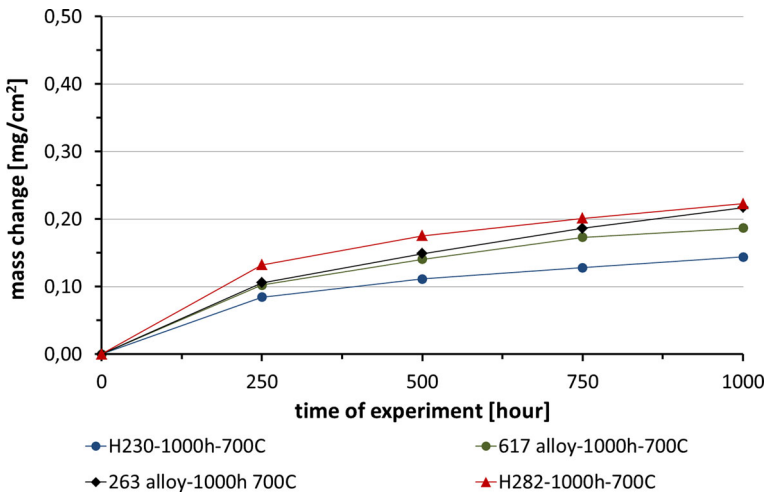


Fig. 2 Kinetic data of the Ni-based alloys exposed to steam oxidation regime at 700 °C for 1000 h

Table 2 Comparison of mass gain at 700 and 800 °C for 1000 h

Material	1000 h 700 °C mass gain (mg/cm ²)	1000 h 800 °C mass gain (mg/cm ²)
310S	0.26	0.50
309S	0.31	0.54
HR3C	0.32	0.57
Haynes [®] 230 [®]	0.14	0.38
Alloy 617	0.19	0.51
Alloy 263	0.22	0.75
Haynes [®] 282 [®]	0.22	0.80

derogations result primarily from the lack of an isothermic condition the initial stage of the high-temperature process (so-called transient oxidation), process as well as the fact that the rate of oxidation of the metal under conditions of direct contact of its surface with air (oxygen) can be much lower than the rate of migration of oxygen atoms to the surface. In addition fractional n factor observed in this work is attributed to complex reaction schemes like chain reactions involving quite a bit of intermediates and free radicals. Hence, it can be suggested that in the case of 309S, 310S and HR3C steels, complex reactions are involved, where transient oxidation initiated every new reaction within the formed oxide scale influence the final n factor value.

Finally, it needs to be pointed out, that during the 1000 h test, mass loss due to the formation of volatile Cr oxyhydroxide has not been observed. The observations are in good agreement with work carried out by Young et al. [8]. The researchers suggested that chromium volatilisation rates from chromia-rich scales can occur under higher pressures, where the partial pressure of oxygen is much higher. In this

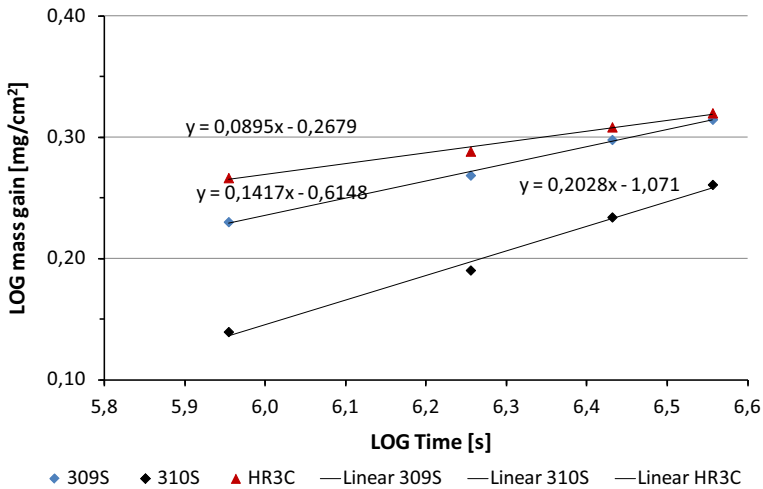


Fig. 3 A plot of log mass gain versus log time to determine the exponent n factor for Fe-based alloys

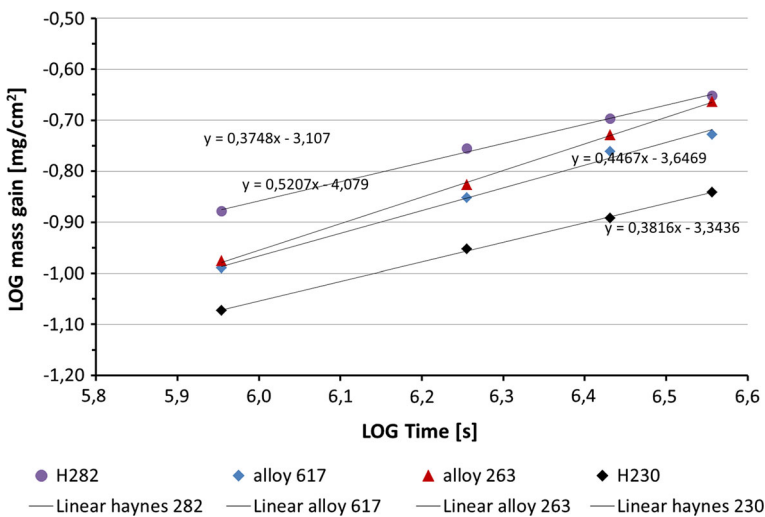


Fig. 4 A plot of log mass gain versus log time to determine the exponent n factor for Ni-based alloys

work, a steam pressure of only 1 bar was used; hence, the partial pressure of oxygen was too low to induce an evaporation reaction.

SEM Observations

Advanced Stainless Steels

Figure 5 shows the cross-sectional morphology of 309S steel developed under steam oxidation at 700 °C for 1000 h. The BSE images captured by SEM show a

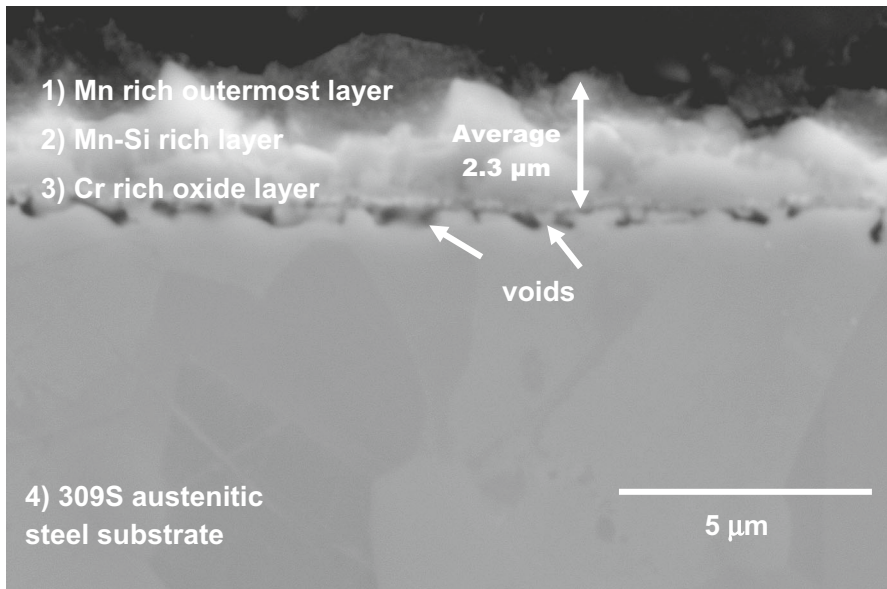


Fig. 5 Cross-sectional microstructure developed under steam oxidation process at 700 °C for 1000 h on 309S steel in steam conditions

double-layered structure of the oxide, with an average thickness of around 2.3 μm ($\sigma = 0.65$), and further, the coefficient of variation (CV) has been measured in order to assess relative variability. In case of 309S steel relative variability showed 6.5%, in overall the values between 0 and 20% indicating small relative variability. The formed oxide scale showed the formation of the outermost layer rich in Mn (55 wt%), and the inner part was rich in Mn and Si with concentrations of 35 and 20 wt%, respectively. Finally, the oxide scale–substrate layer was enriched in Cr, with around 40 wt% of Cr suggesting the formation of a Cr–O oxide. According to EDS concentration profiles (wt%) for the exposed 309S austenitic steel shown in Fig. 6, the oxide scale can be divided into four different sections: the outermost 0.5 μm thick oxide layer, a 1.5 μm thick middle layer with enriched Mn and Si content, a 1 μm enriched Cr layer and finally, the substrate. Underneath the oxide scale, in the oxide scale–substrate interface subsurface voids were found. The presence of these subsurface voids with dimensions of 0.1–0.5 μm may have derived from pull out during polishing or the subsurface voids may have formed under the steam oxidation process. To explain the problem, FIB equipment should be used to perform a cross-cutting process throughout the formed oxide scale in order to understand the problem in more detail. Microscopic observations revealed that the oxide scale developed under the steam oxidation process in 309S steel at 700 °C showed good adherence to the substrate with no spallation or detachment, subsurface voids, as mentioned previously formed in the oxide scale–the substrate interface.

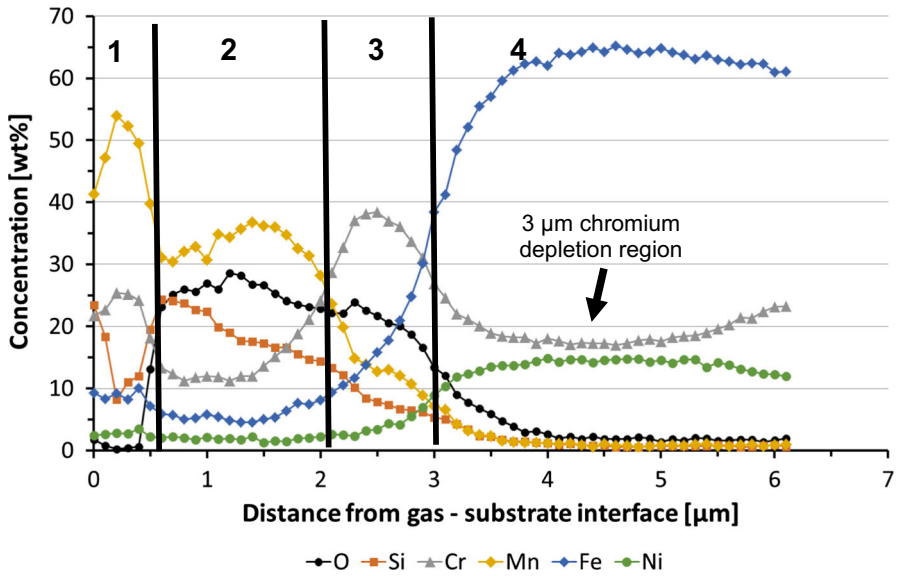


Fig. 6 Concentration profiles captured from cross-sectioned steel 309S exposed at 700 °C for 1000 h

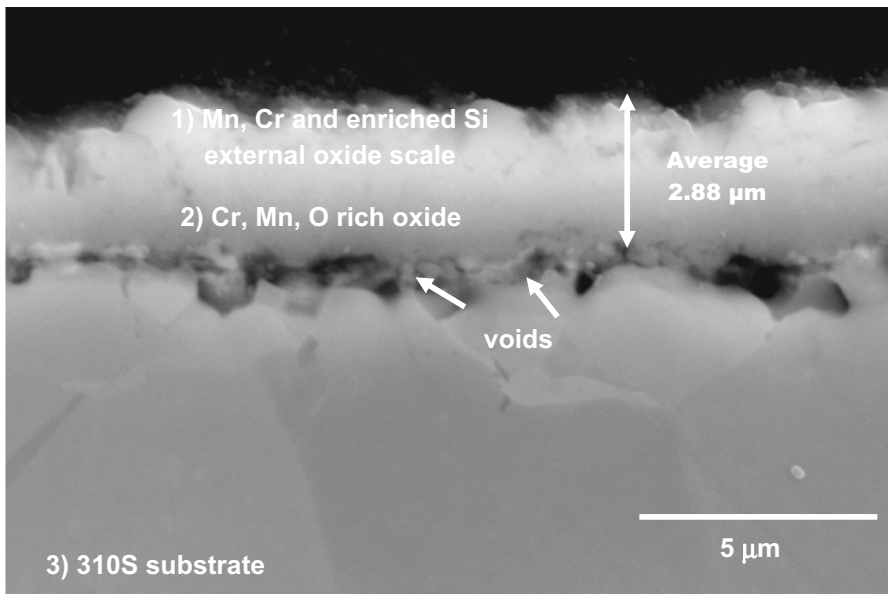


Fig. 7 Cross-sectional microstructure developed under steam oxidation process at 700 °C for 1000 h on 310S steel in steam conditions

In contrast to 309S steel, the cross-sectioned SEM image presented in Fig. 7 indicates that steam oxidation of 310S steel leads to the development of an oxide scale with an average thickness of $2.85\ \mu\text{m}$, ($\sigma = 0.62$), and low relative variability equivalent to 6.2%. The most external $0.3\ \mu\text{m}$ thick oxide scale consists of mainly Cr (50 wt%), Mn (15 wt%), O (20 wt%) and Si (10 wt%). Other elements like Fe and Ni showed negligible concentrations of less than 5 wt%. The second layer within the developed oxide scale was enriched in Cr (55 wt%) with a stable and constant concentration of Mn, Si and Fe according to the EDS concentration profile is shown in Fig. 8. Similar to 309S steel, the material show no crack, delamination and other defects of the oxide scale; however, between the metallic core and the oxide scale voids formed, the subsurface voids had a bigger dimension than that found in 309S steel reaching up to $0.8\text{--}1\ \mu\text{m}$.

The steel with the highest Cr concentration (25 wt%) showed the development of thin oxide scale as is shown in Fig. 9. The oxide scale with average thickness of $1.86\ \mu\text{m}$, ($\sigma = 0.044$), low relative variability equivalent to 4.4%, suggesting more uniform and flat oxide microstructure than that developed in 309S and 310S steels, respectively. According to EDS concentration profiles in Fig. 10, the oxide scale showed much lower concentration of Mn compared to the 309S and 310S steels, respectively; however, HR3C steel presented similar concentration of Cr (55 wt%) than that observed in 310S steel and much higher Cr concentration of Cr than that in

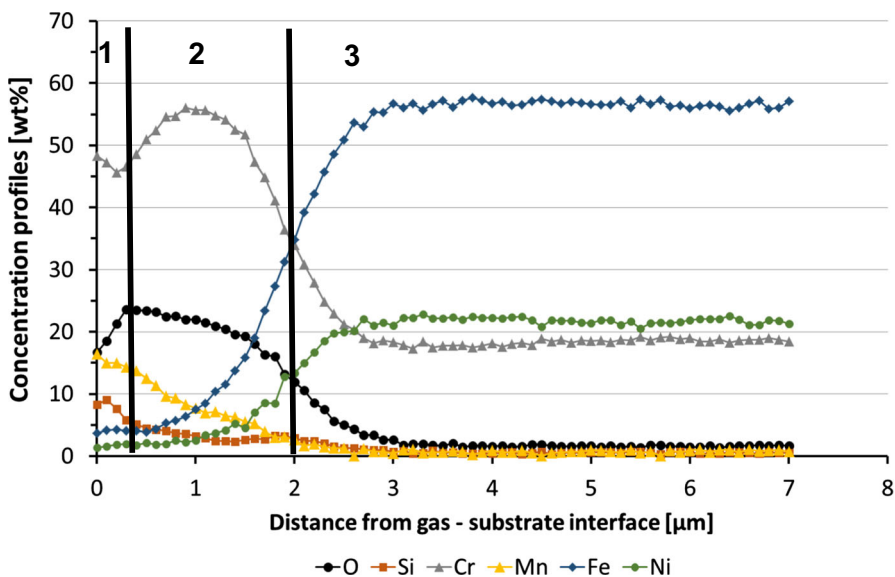


Fig. 8 Concentration profiles captured from cross-sectioned steel 310S exposed at $700\ \text{°C}$ for 1000 h in steam conditions

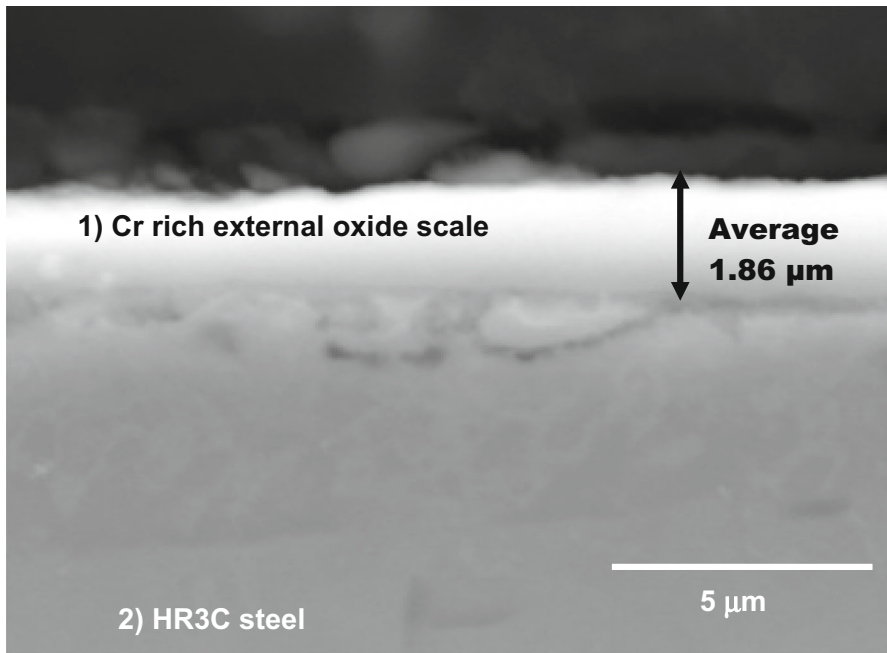


Fig. 9 Cross-sectional microstructure developed under steam oxidation process at 700 °C for 1000 h on HR3C steel

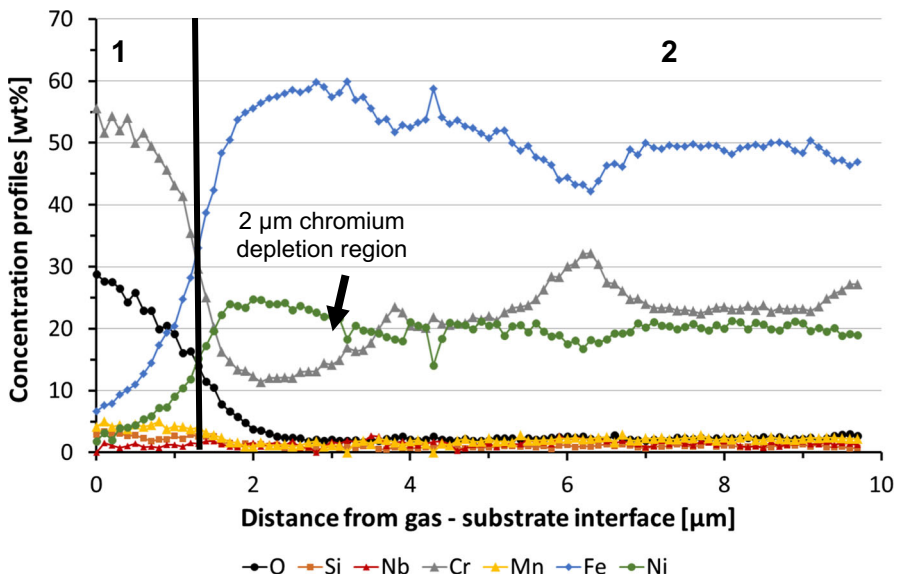


Fig. 10 Concentration profiles captured from cross-sectioned steel HR3C exposed at 700 °C for 1000 h in steam conditions

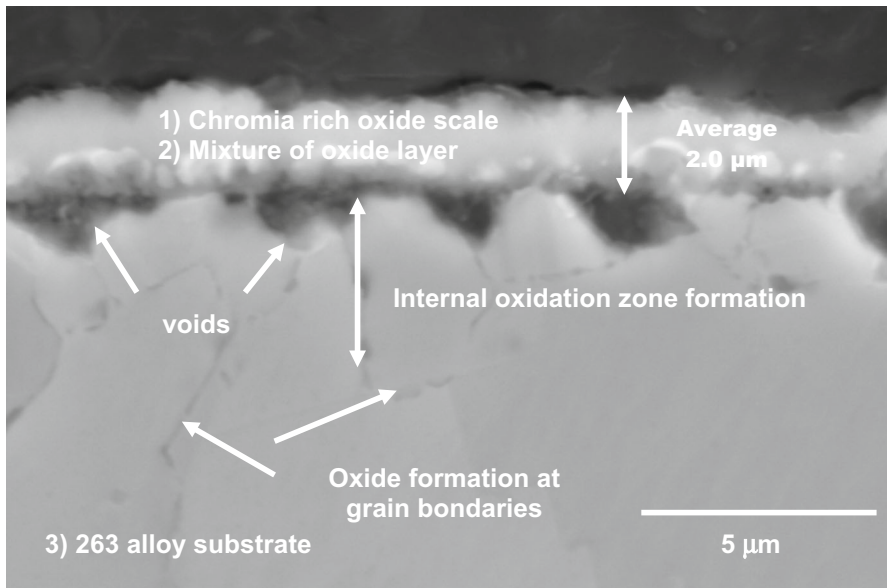


Fig. 11 Cross-sectional microstructure of the 263 alloy exposed to steam at 700 °C for 1000 h

309S steel (25 wt%). Underneath the oxide scale, 2 μm in length Cr depletion region formed due to outward diffusion of Cr has been observed.

Ni-Based Alloys

Figure 11 presents a cross-sectioned SEM picture of 263 alloy exposed to steam oxidation conditions. The alloy developed a thin oxide scale with an average thickness of 2.3 μm, ($\sigma = 0.13$) and low relative variability equivalent to 13%. The external part of the oxide scale with a thickness of around 1 μm was rich in Cr (70 wt%) with addition of Ni (10 wt%) and Ti (10 wt%). The total concentration of other elements reached around 10 wt%. The second layer with the oxide scale showed enrichment in Ni and a lowered concentration of Cr in addition to a slightly lower concentration of Ti (7 wt%). Underneath the oxide scale, a Cr depletion zone around 2 μm thick was formed according to the results shown in Fig. 12, where EDS concentration profiles versus distance from gas–surface interface in μm are shown. In comparison with austenitic steel, 263 alloy showed the formation of large voids with dimension of 1.5 μm in diameter. The cross-sectioned SEM image in BSE mode of 617 alloy after steam exposure at 700 °C for 1000 h is shown in Fig. 13. The exposure induced the formation of a much thinner oxide scale, with an average value of 1.1 μm, ($\sigma = 0.079$), and low relative variability equivalent to 7.9% indicating flat, oxide scale microstructure. Furthermore, in contrast to 263 alloy, 617 alloy developed a single-phase oxide scale consisting of Ni, Cr and O, suggesting the formation of NiCr₂O₄ spinel. Similar to the 263 alloy, underneath a

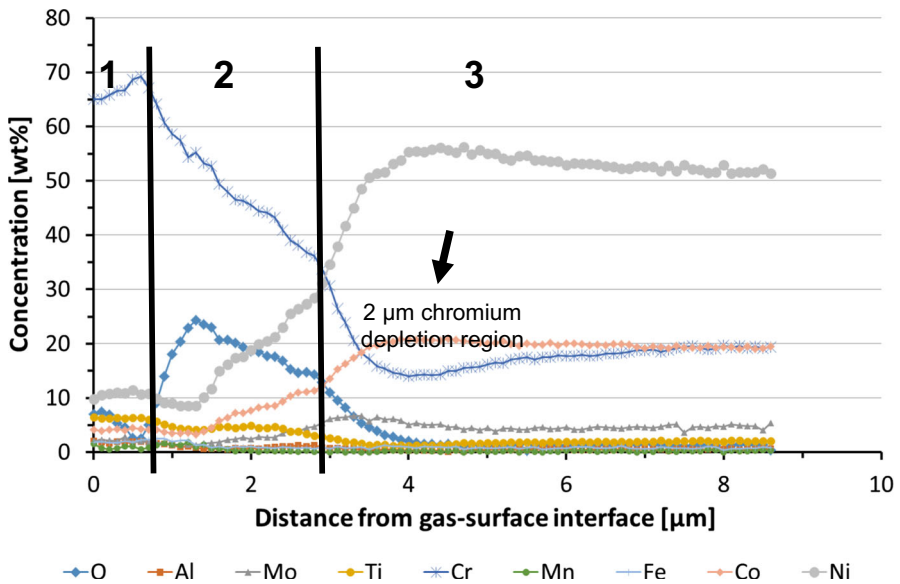


Fig. 12 Concentration profiles captured from cross-sectioned Ni-based 263 alloy exposed at 700 °C for 1000 h in steam conditions

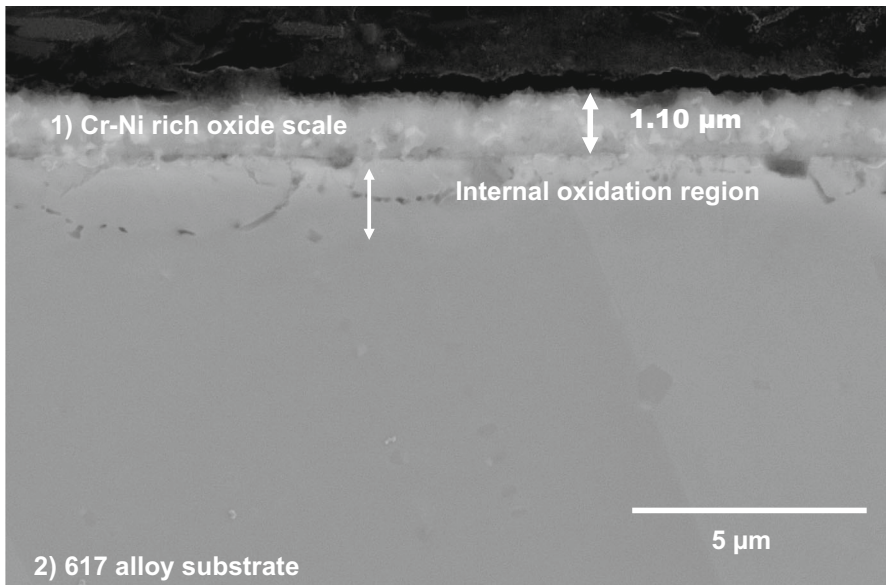


Fig. 13 Cross-sectional microstructure of the 617 alloy exposed to steam at 700 °C for 1000 h

thin oxide scale, 2.5 μm thick Cr depletion zone according to EDS shown in Fig. 14 was observed.

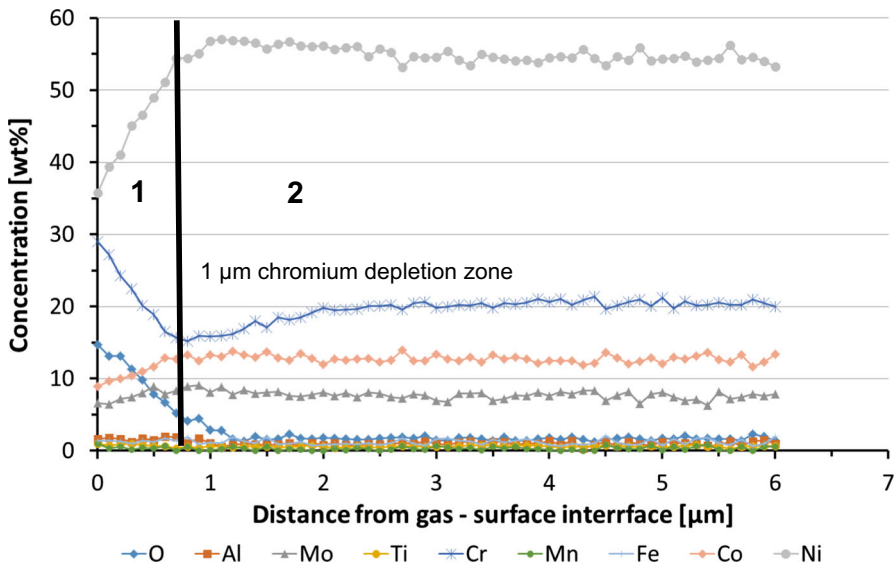


Fig. 14 Concentration profiles captured from cross-sectioned Ni-based 617 alloy exposed at 700 °C for 1000 h in steam conditions

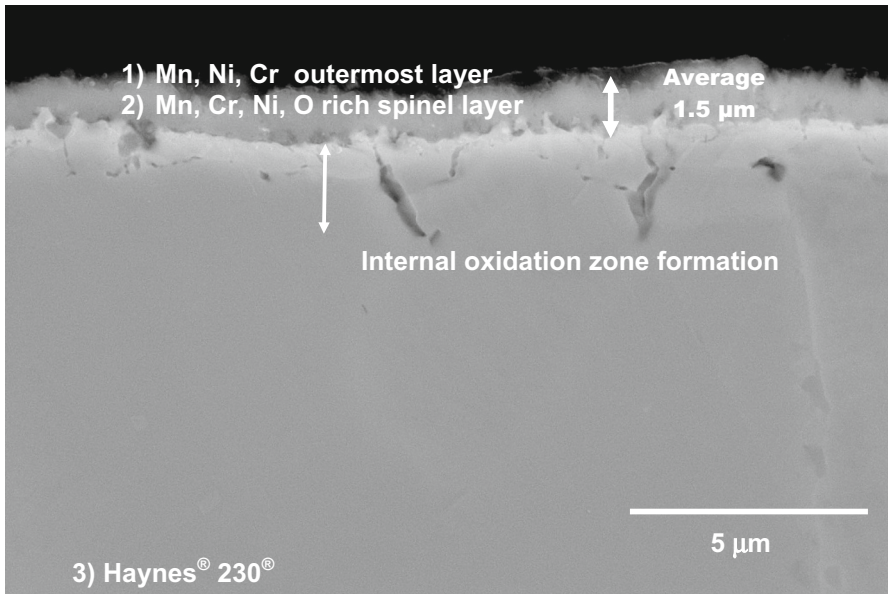


Fig. 15 Cross-sectional microstructure of the Haynes® 230® exposed to steam at 700 °C for 1000 h

The Ni-based 617 alloy underwent a similar internal oxidation process to 263 alloy, the oxidation reached 1.5 μm deep inside the material indicating a much lower degree of internal oxidation process than that which was observed in 263

alloy. Furthermore, in comparison with 263 alloy, 617 alloy shows no Ti enrichment within the oxide scale. The enrichment may influence kinetics due to the formation of a sublayer packed with TiO_2 phase underneath the rich Cr oxide scale, as was observed in the 263 alloy.

The cross-sectioned SEM image in BSE mode of Haynes[®] 230[®] Ni-based alloy is shown in Fig. 15. An average thickness measured from 10 different measurements (similar to other alloys in this work) indicates that thickness reached an average value of 1.63 μm , ($\sigma = 0.05$) and low relative variability equivalent to 5%. The microscopic observations revealed that the alloy developed the an external scale consisting of Cr (60 wt%), Mn (8 wt%) and finally O (20 wt%) with a thickness of 0.5 μm . Underneath the external scale, a thin and an adherent oxide scale with lowered Cr content (50 wt%), lowered Mn content (5 wt%) higher O content (25 wt%) was observed. The thickness of the second layer reached around 1 μm according to EDS concentration profiles is shown in Fig. 16.

The highest corrosion degradation under steam oxidation conditions was observed in Haynes[®] 282[®] Ni-based alloy. The alloy developed an oxide scale with an average value of 1.8 μm , ($\sigma = 0.066$), and low relative variability equivalent to 6.6% indicating (similar to other materials exposed in this work) rather smooth, flatten oxide scale microstructure. The outermost part of the oxide scale according to EDS concentration profiles in Haynes[®] 282[®] consisted of a high concentration of Cr (almost 65 wt%) and a similar concentration of Ti and Ni (around 7 wt%). In contrast to other Ni-based alloys, Haynes[®] 282[®] presented the development of a thick Cr depletion zone (5 μm) as indicated by EDS elemental distribution is shown in Fig. 18. Furthermore, cross-sectioned microscopic SEM

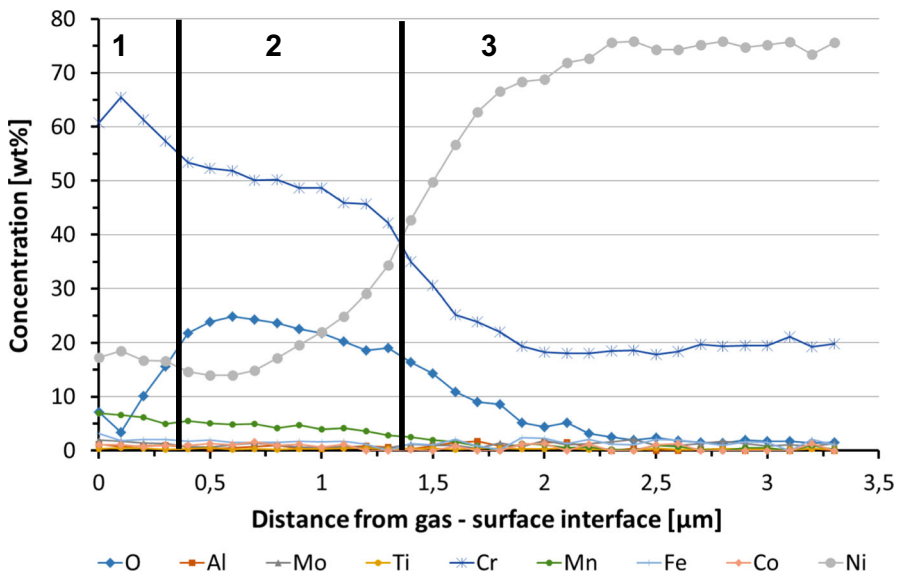


Fig. 16 Concentration profiles captured from cross-sectioned Ni-based Haynes[®] 230[®] alloy exposed at 700 °C for 1000 h in steam conditions

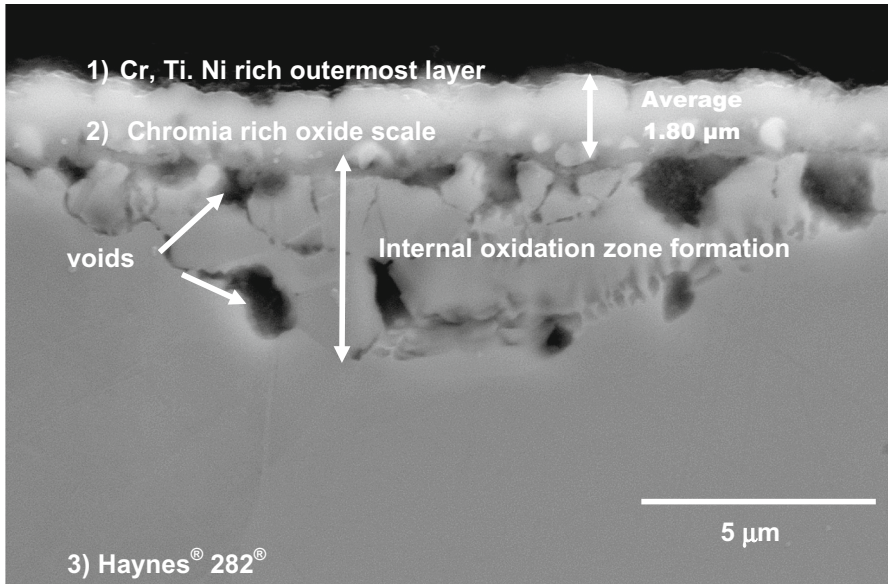


Fig. 17 Cross-sectional microstructure of the Haynes® 282® exposed to steam at 700 °C for 1000 h

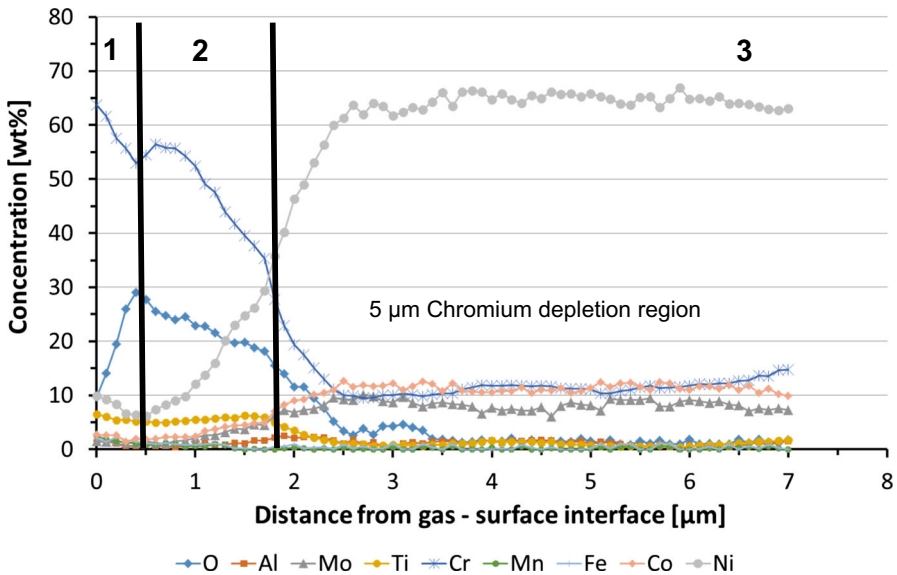


Fig. 18 Concentration profiles captured from cross-sectioned Ni-based Haynes® 282® alloy exposed at 700 °C for 1000 h in steam conditions

imaging carried out in BSE mode revealed that Haynes® 282® Ni-based alloy showed the development of a high number of subsurface voids with dimensions of 1–2.5 μm together with the highest degree of internal oxidation (Fig. 17).

Fig. 19 XRD pattern for advanced austenitic steels exposed to 700 °C for 1000 h: **a** 309S, **b** 310S, and **c** HR3C

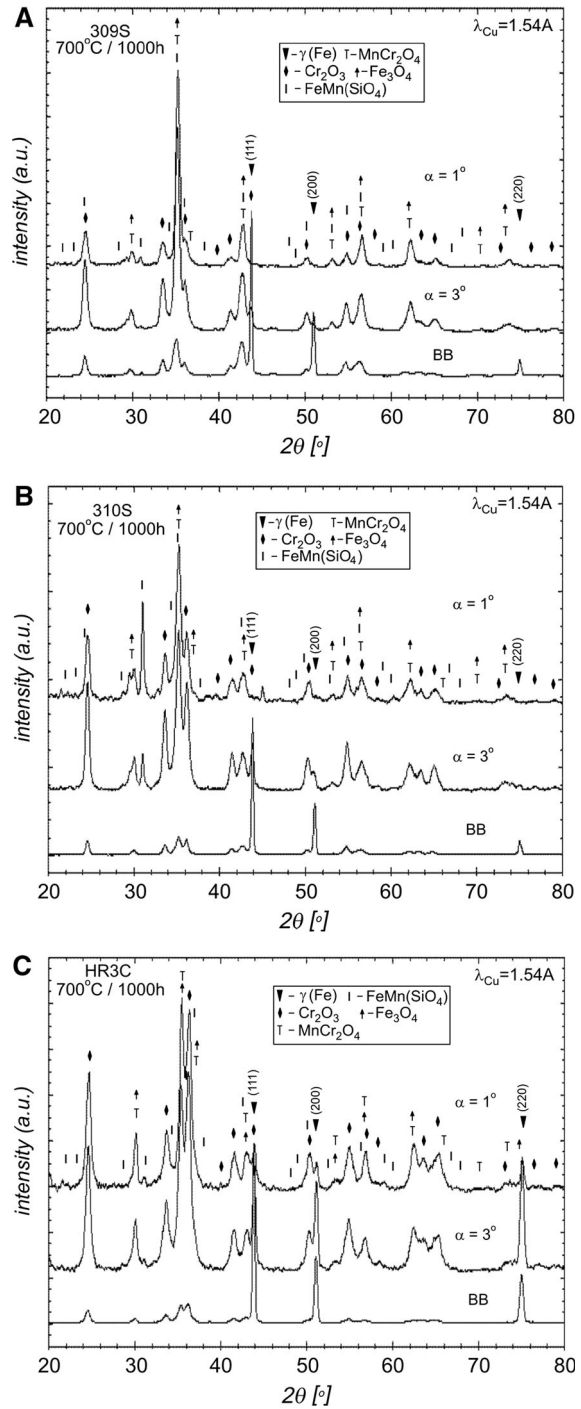


Table 3 Phase developed under steam oxidation at 700 °C for 1000 h for austenitic steels: + 1 indicates the most dominating phase, + 2, the second most dominating phase and + presence of a phase

Material	Time (h)	Geom.	Cr ₂ O ₃	MnCr ₂ O ₄	FeMn(SiO ₄)	Fe ₃ O ₄
310S	1000	BB	+ 2	+ 1	+	+ 1
		$\alpha = 3^\circ$	+ 2	+ 1	+	+ 1
		$\alpha = 1^\circ$	+	+ 1	+ 2	+ 1
309S	1000	BB	+ 2	+ 1	+	+ 1
		$\alpha = 3^\circ$	+ 2	+ 1	+	+ 1
		$\alpha = 1^\circ$	+ 2	+ 1	+	+ 1
HR3C	1000	BB	+ 1	+ 2	+	+ 2
		$\alpha = 3^\circ$	+ 1	+ 2	+	+ 2
		$\alpha = 1^\circ$	+ 2	+ 1	+	+ 1

XRD Analyses

The XRD studies in this work were conducted for better traceability of the corrosion process in steam conditions for 1000 h at 700 °C. The studies were performed in three different modes in order to investigate more accurately the phase composition of the formed oxides. The exposed materials were investigated using two techniques: Bragg–Brentano (BB) geometry and the geometry of constant angle called grazing incidence using $\alpha = 1^\circ$ and $\alpha = 3^\circ$. Figure 19a–c presents XRD patterns for stainless steels and Ni-based alloys with high Cr concentrations. As shown, the steels developed four principal compounds: Cr₂O₃, MnCr₂O₄, FeMn(SiO₄) and finally Fe₃O₄. In the case of 309S, 310S, the outermost oxide scale layer investigated using constant angle called grazing incidence using $\alpha = 1^\circ$ consisted of mostly MnCr₂O₄, Fe₃O₄ and a tiny quantity of Cr₂O₃. When a constant angle $\alpha = 3^\circ$ and BB mode was used, a stronger peak of Cr₂O₃ was identified besides the MnCr₂O₄, FeMn(SiO₄) and Fe₃O₄ in both 309S and 310S stainless steel materials. In the HR3C material with the highest Cr concentration, the outermost layer of the oxide scale contained mostly of MnCr₂O₄ and Fe₃O₄; however, within the formed oxide scale the majority quantity was identified as Cr₂O₃. In BB mode, Cr₂O₃ was the most dominating compound observed using XRD investigations. For better traceability of the archived results, Table 3 shows the phases observed under XRD investigations. Furthermore, in comparison with the study performed earlier [6], at 700 °C, the following phases were not detected in stainless steels: SiO₂, Mn₇SiO₁₂, and Cr₃O₄. The XRD diffraction patterns for Ni-based alloys exposed at 700 °C for 1000 h are shown in Fig. 20a–d.

According to the results, the Ni-based alloys exposed in this study developed mainly Cr₂O₃, and MnCr₂O₄ spinel phases in case of 263 alloy, Haynes[®] 230[®], and Haynes[®] 282[®]. In addition, due to the formation of a thin oxide scale on Haynes[®] 230[®], the XRD pattern shown as well double carbides, η : Co₃W₃C and Co₆W₆C. In the 617 alloy instead of a MnCr₂O₄ spinel, an NiCr₂O₄ phase developed, since the 617 alloy showed no Mn concentration within the metal matrix. In comparison to the study performed at higher temperatures [6] only gamma-prime (γ') strengthened

Fig. 20 XRD pattern for Ni-based alloys exposed to 700 °C for 1000 h: **a** 263 alloy, **b** 617 alloy, **c** Haynes[®] 230[®], and **d** Haynes[®] 282[®]

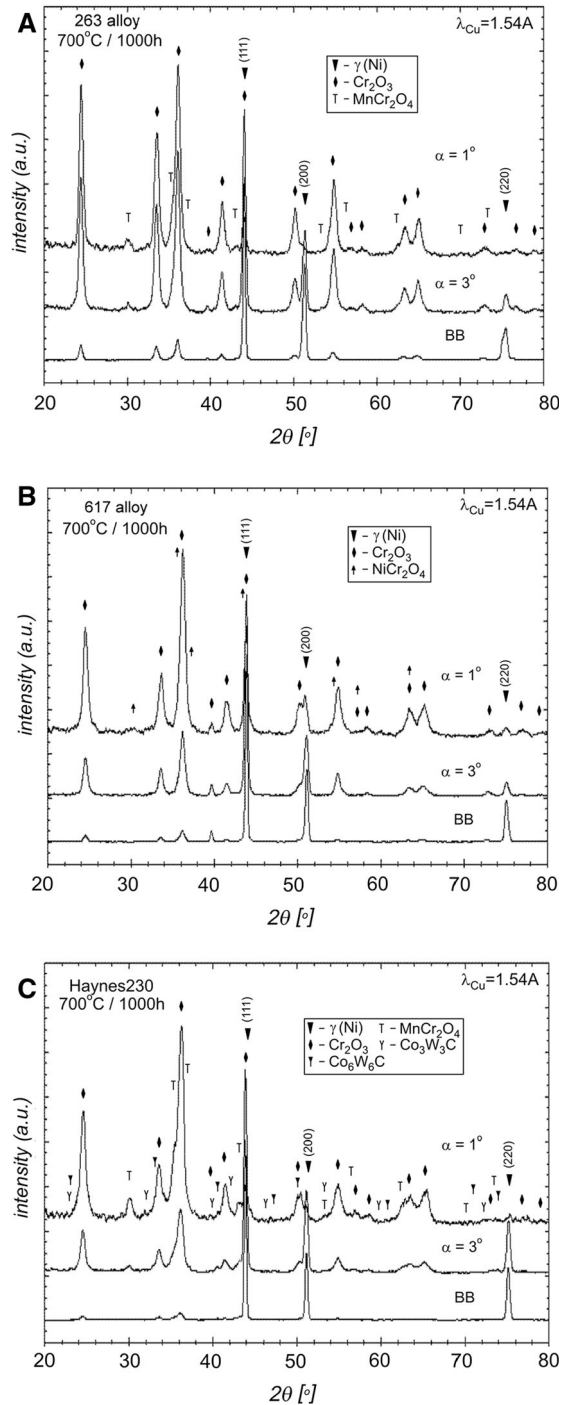


Fig. 20 continued

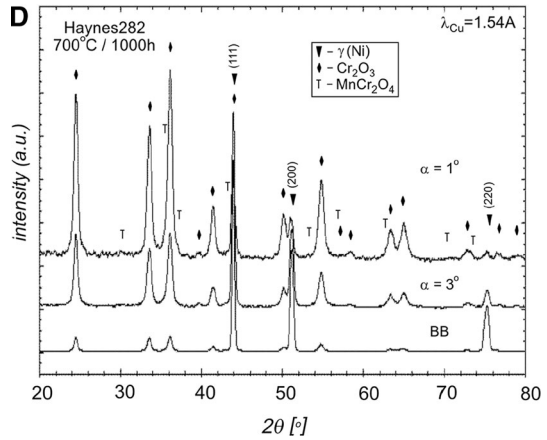


Table 4 Phase developed under steam oxidation at 700 °C for 1000 h for Ni-based alloys: + 1 indicates the most dominating phase, + 2, the second most dominating phase, t denotes trace quantity and + presence of a phase

Material	Time (h)	Geom.	Cr ₂ O ₃	MnCr ₂ O ₄	NiCr ₂ O ₄	Co ₃ W ₃ C	Co ₆ W ₆ C
263 alloy	1000	BB	+ 1	+ 2			
		$\alpha = 3^\circ$	+ 1	+ 2			
		$\alpha = 1^\circ$	+ 1	+ 2			
617 alloy	1000	BB	+ 1		+ 2t		
		$\alpha = 3^\circ$	+ 1		+ 2t		
		$\alpha = 1^\circ$	+ 1		+ 2t		
Haynes [®] 230 [®]	1000	BB	+ 1	+ 2		+	+
		$\alpha = 3^\circ$	+ 1	+ 2		+ t	+ t
		$\alpha = 1^\circ$	+ 1	+ 2		+ t	+ t
Haynes [®] 282 [®]	1000	BB	+ 1	+ 2t			
		$\alpha = 3^\circ$	+ 1	+ 2t			
		$\alpha = 1^\circ$	+ 1	+ 2t			

Ni-based alloys showed a difference in phase development due to the lack of formation of TiO₂ and MnTiO₃ compounds. The Ni-based solid solution strengthened alloys developed the same phases as was reported in the work published earlier [6], despite 0.3 wt% Ti in the 617 alloy, no Ti containing phase was observed on XRD pattern. It is suggested that development of Ti containing phases is related strongly to concentration, activity, temperature and perhaps volume. For better clarity of the results, Table 4 shows a summary of the XRD investigations performed on Ni-based alloys exposed at 700 °C for 1000 h.

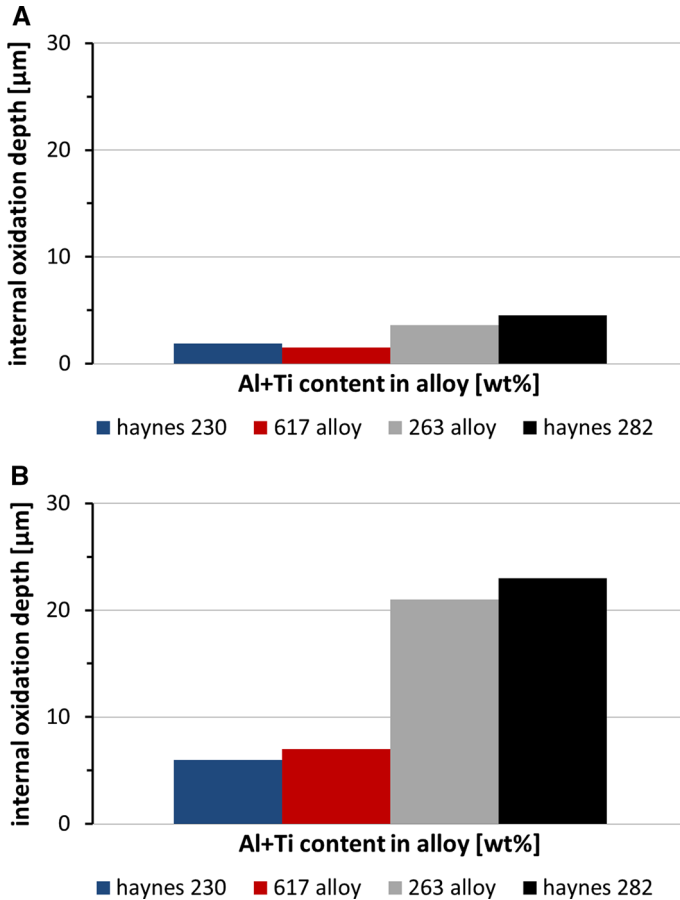


Fig. 21 A comparison of internal oxidation depths at 700 and 800 °C for 1000 h in steam conditions

Discussion

Due to the large number of samples and results achieved in this work, the discussion section is divided into three subsections called: Ni-based alloys, austenitic steels and voids formation.

Ni-Based Alloys

Corrosion resistance of Ni-based alloys exposed at 700 °C for 1000 h is attributed mainly to the formation of a rich Cr_2O_3 external oxide scale. The highest performance was found to be in Haynes[®] 230[®] alloy amongst the Ni-based alloys exposed in this work, the lowest performance was found to be in Haynes[®] 282[®]. Similarly to work performed earlier [6], two solid solution strengthened alloys; Haynes[®] 230[®] and 617 alloy showed lower weight gain than two gamma-prime (γ') strengthened alloys; 263 alloy and Haynes[®] 282[®]. Nevertheless, in contrast to

previous study [6], there is no strict evidence for the formation of TiO_2 , however mass gain of two gamma-prime (γ') strengthened alloys is higher than that observed for two solid solution strengthened Ni-based alloys, hence it is suggested that the higher mass gain is attributed to a higher degree of internal oxidation found in gamma-prime (γ') strengthened alloys. The exposed Ni-based alloys underwent a different degree of internal oxidation, however, much lower than that observed at 800 °C [6], as shown in Fig. 21.

The lowest degree was found to be in alloy 617 and Haynes[®] 230[®] where the addition of Ti and Al to the alloy metal matrix was the lowest. The highest degree of internal oxidation process corresponds to the Ni-based alloy with the highest Ti and Al concentration in the metal matrix (Haynes[®] 282[®]). Hence, the presence of Ti and Al in the Ni-based metal matrix increases susceptibility to internal oxidation processes at high temperatures in steam environments.

Austenitic Steels

The advanced steels rich in Cr with tiny amounts of Si, in comparison to Ni-based alloys exposed at 700 °C for 1000 h, showed slightly better corrosion resistance in terms of weight gain, scale structure and internal oxidation process. Firstly, the exposed steels showed no internal oxidation zone formation at 700 °C. The observed corrosion resistance was attributed mainly to the formation of rich Cr_2O_3 and MnCr_2O_3 oxide scales with a sublayer containing $\text{FeMn}(\text{SiO}_4)$ according to findings from XRD studies. In contrast to the study performed on the same batch of materials at 800 °C for 1000 h, an Fe_3O_4 phase was found in every stainless steel exposed in this study; however, at 800 °C only HR3C steel showed the development of an Fe_3O_4 phase. The role of those oxides in high-temperature corrosion has been discussed previously [9, 10]. Briefly, Henry et al. [11], observed that with an increasing Si content from 0 to 1 wt%, in 15 wt% Cr steel, it induces prolongation of breakaway oxidation from 2 to more than 50 h. In this study, the addition of Si to 309S and 310S steels (with > 20 wt% Cr) enhanced the breakaway oxidation process, not only because of high Cr content and the formation of stable Cr_2O_3 , but also due to the effect of Si. The 309S and HR3C steels with the same Si concentration (0.75 wt%) showed almost the same mass gain despite the higher Cr content in HR3C steel than in 309S steel. Hence, it can be concluded that the effect of Si is clearly observed under tested conditions. The same mechanism has been found by Ishitsuka et al. [12] in low Cr steel (T91) where the addition of Si significantly enhanced oxidation resistance due to the formation of an amorphous SiO_2 sublayer. In this case along with amorphous SiO_2 , the process is attributed to the development of an $\text{FeMn}(\text{SiO}_4)$ phase in 310S steel as the second most dominating phase. It is believed that the formation of $\text{FeMn}(\text{SiO}_4)$ phase positively influences kinetic behaviour at 700 °C. The exposed steels, similar to Ni-based alloys, show no evaporation of Cr from Cr_2O_3 , and the three steels developed a MnCr_2O_4 spinel within the oxide scale in addition to a Cr_2O_3 phase.

Voids Formation

The study performed in this research showed that Fe- and Ni-based alloys underwent a corrosion process. It has been found based on cross-sectioned images, that the steels (309S, 310S) and Ni-based alloys (263 alloy and Haynes[®] 282[®]) indicated the development of subsurface voids underneath the oxide scale at the interface. The formation of voids and location of voids strongly depends from transport mechanism. In this work in 309S, 310S steels and in 263 alloy and Haynes[®] 282[®] mass transport occurred via vacancy diffusion mechanism, this mechanism is closely related to the formation of vacancies induced by the subsurface diffusion of Cr from metal matrix to form rich Cr oxide scale [13]. In general, number of voids in subsurface increases with time and decreases with depth. Furthermore, similar to work published earlier [13], in this work voids are only observed in Cr depleted region. Another mechanism for voids formation have been described by Stott et al. [14], and Juana et al. [15] suggesting that the phenomena is related strictly to the breaking mechanism of the oxide scale in pure steam at 700 °C. The breakaway of this protective chromia scale formed in steam may be related to the hydrogen permeability and diffusion of Mn to the Cr₂O₃. The growth of scale is mainly supported by the outward diffusion of chromium ions and usually occurs via a vacancies gradient, which, when injected into the metal substrate, causes a vacancy supersaturation and eventually condenses as voids. The hydrogen may move into the voids at the scale interface which usually acts as hydrogen trap. The increasing pressure in the voids would promote the buckling of the protective chromia scale. Once the chromia scale cannot relieve the stress by deformation, cracks occur. After a short time exposure, the chromium concentration in the steel near the scale interface is sufficient to heal the protective chromia scale. After a longer exposure, more chromium is lost by repeated cracking and healing, and the decreased chromium content in the steel near the outer surface cannot sustain the healing of protective chromia scale. The iron in the steel therefore oxidises rapidly and forms the crater structure [3]. Scale failure at high temperatures is also caused due to relatively rapid rates of diffusion of manganese across the Cr and O scale and the formation of a Mn–Cr spinel on its outer surface. The scale consists of a layer of Cr₂O₃, containing a small concentration of manganese, with an outer layer of the spinel oxide. During the early stages, an inner layer of the spinel also develops, but, eventually, this almost completely disappears as the manganese diffuses into the outer scale according to work describe by Stott et al. [14].

Similar voids have also been observed in Ni-based alloys, but only in the 263 alloy and Haynes[®] 282[®] materials, those alloys had the highest Ti concentrations (1.2 and 2.1 wt% Ti, respectively). Based on the results it can be suggested that the formation of larger voids underneath the oxide scale in Ti rich Ni-based alloys is invoked not only by process described by researchers [13, 14, 1415] but can be enhanced further by oxygen vacancies existing in the TiO₂ phase that formed here, however, for analytical instruments used in this study it was unreachable.

Conclusions

The aim of this paper was to perform steam oxidation tests for 1000 h at 700 °C of the rich Cr austenitic steels: 309S, 310S and HR3C, Ni-based alloys: 617 alloy, Haynes® 230®, 263 alloy, and finally Haynes® 282®. The results obtained indicated that the steel and Ni-based alloys showed much lower mass gain than that observed at higher temperatures (800 °C). Furthermore, the Ni-based alloys showed lowered internal oxidation rates. Both types of material showed no evaporation of the Cr phase.

At 700 °C compared to tests carried out at 800 °C, no TiO₂ formation was observed. Finally the exposed materials developed mainly: Cr₂O₃ and MnCr₂O₄ phases. 617 alloy showed the formation of a NiCr₂O₄ phase. The austenitic steels containing up to 1.5 wt% Si developed a phase containing Si: FeMn(SiO₄). Finally, both types of materials developed subsurface voids via vacancy injection induced by the subsurface diffusion of chromium to form a surface oxide Cr₂O₃.

Acknowledgements The authors would like to acknowledge National Science Centre in Poland for the financial support of the fundamental research under the project number 2014/13/D/ST8/03256. Furthermore, the authors would like to acknowledge the following materials providers: Haynes International, Sandmeyer Steel Company and finally Institute for Ferrous Metallurgy in Poland for Ni-based and advanced steels supply.

Open Access This article is distributed under the terms of the Creative Commons Attribution 4.0 International License (<http://creativecommons.org/licenses/by/4.0/>), which permits unrestricted use, distribution, and reproduction in any medium, provided you give appropriate credit to the original author(s) and the source, provide a link to the Creative Commons license, and indicate if changes were made.

References

1. Technology Roadmap High-Efficiency, Low-Emissions Coal-Fired Power Generation: International Energy Agency (IEA), (2012).
2. I. Wright, A. Sabau and R. Dooley, *Materials Science Forum* **595–598**, 387 (2008).
3. E. Essuman, L. R. Walker, P. J. Maziasz and B. A. Pint, Oxidation behaviour of cast Ni–Cr alloys in steam at 800 °C. *Materials Science and Technology* **29**, 822 (2013).
4. Lee M. Pike and S. K. Srivastava, Oxidation Behavior of Wrought Gamma-Prime Strengthened Alloys. *Materials Science Forum* **595–598**, 661 (2008).
5. J. Young, *Chapter 6 Oxidation of Alloys II: Internal Oxidation, High Temperature Oxidation and Corrosion of Metals, Corrosion Series*, Vol. 1, (Elsevier, Amsterdam, 2008), p. 247.
6. T. Dudziak, V. Deodshumukh, L. Backert, N. Sobczak, M. Witkowska, W. Ratuszek, K. Chruściel, A. Zieliński, J. Sobczak and G. Bruzda, *Oxidation of Metals* **87**, 1398 (2016).
7. B. Pieraggi, *Oxidation of Metals* **27**, (3), 177 (1986).
8. D. J. Young and B. A. Pint, *Oxidation of Metals* **66**, 137 (2006).
9. A. Fry, S. Osgerby and M. Wright, *Oxidation of Alloys in Steam Environments—A Review*, (NPL, London, 2002).
10. N. K. Othman, N. Othman, J. Zhang and D. J. Young, *Corrosion Science* **51**, 3039 (2009).
11. S. Henry, A. Galerie and L. Antoni, *Materials Science Forum* **369–372**, 353 (2001).
12. T. Ishitsuka, Y. Inoue and H. Ogawa, *Oxidation of Metals* **61**, 125 (2004).
13. *Mechanical Properties of Metallic Composites*, ed. S. Ochiai (Marcel Dekker Inc., New York, 1994).
14. F. H. Stott, F. I. Wei and C. A. Enahoro, *Materials and Corrosion* **40**, 198 (1989).
15. J. Yuana, W. Wangb, H. Zhangb, L. Zhua, S. Zhub and F. Wangb, *Corrosion Science* **109**, 36 (2016).